Journal of Applied Polymer Science

Understanding the Effects of Nanocarbons on Flexible Polymer Chain Orientation and Crystallization: Polyethylene/Carbon Nanochip Hybrid Fibrillar Crystal Growth

Emily C. Green, Yiying Zhang, Marilyn L. Minus
Department of Mechanical and Industrial Engineering, Northeastern University, Boston, Massachusetts 02115-5000
Correspondence to: M. L. Minus (E-mail: m.minus@neu.edu)

ABSTRACT: Polyethylene (PE)/carbon nanochip fibers (CNCF) fibrillar crystals were grown under shear flow. The fibrillar crystals ranged from 25 to 200 nm in diameter and bundled to form PE/CNCF macro-fibers. The PE/CNCF fibers were further processed by hot-drawing near the PE melting temperature. On the basis of small-angle X-ray analysis, it was found that during drawing the presence of CNCF led to continuous extended-chain PE crystal growth. DSC melting peaks associated with transformation of the orthorhombic to a hexagonal lattice phase in the PE crystal structure (i.e., increased ordering and extension of the polymer chain along the fiber axis) was also observed for drawn hybrid PE/CNCF fibrillar crystals. The orientation factor for the extended-chain (i.e., shish) crystals in the hybrid as compared to the control fibers improved from 0.88 to 0.93. This work shows the direct evidence that these nanocarbon fillers can promote extended-chain polymer crystal growth under shear. © 2014 Wiley Periodicals, Inc. J. Appl. Polym. Sci. **2014**, *131*, 40763.

KEYWORDS: composites; crystallization; graphene and fullerenes; nanotubes; polyolefins

Received 14 November 2013; accepted 24 March 2014
DOI: 10.1002/app.40763

INTRODUCTION

Polymer crystallization plays a large role in the physical and chemical properties of a polymer. As such, manipulating polymer crystal growth during the processing of materials has important implications for building specific polymer architectures. Morphological registry and design is important for the processing of polymer nanocomposites in order to control the properties, and this may be accomplished by understanding crystallization in these systems. Nanofillers have been found to influence polymer crystallization,[1–4] in particular carbon nanotubes (CNT) have been shown to template polymer crystallization and orientation.[5,6] A number of mechanisms currently exist for controlling the polymer crystal structure including nucleation,[7,8] solidification[9,10] solution crystallization,[11,13] and crystallization in the presence of nanofillers.[14–16]

This study is focused on understanding the mechanism for inducing extended-chain polymer crystal growth in polymer/nanocarbon composite fibers. Polyethylene (PE) is a benchmark polymer for understanding polymer crystallization.[17–19] The observation of shish (i.e., extended-chain) crystals was first characterized in this system.[11,20] It has also been shown that highly oriented, extended-chain polymers can be achieved under shear flow.[20,21] The resultant crystal morphology obtained through shear flow of PE solution is a shish-kebab structure as evidenced previously.[12,13,22] Extended-chain PE crystals formed under shear-flow make up the shish portion, whereas the kebab portion is made-up of folded-chain PE crystals. In more recent work, shear flow has been used to template PE extended-chain crystals on CNT.[5]

Nanofillers including CNT have received much attention over the past decade due to their superior properties.[23–25] This attention has led to the development of many polymer-nanocomposite materials aimed at utilizing the properties of these fillers. Fundamental understanding of how polymers and nanofillers interact is vital for fabrication of composites with tailored structure and properties. These interactions also provide insight toward interfacial properties in the nanocomposites. Polymer crystallization provides one pathway to understanding these interactions and the potential of influence by the nanocomponent on the polymer.[26–28]

It is now well known that CNT can nucleate the growth of polymer crystals.[7,29,30] In polymer systems with CNT present, a nanohybrid shish-kebab structure has been observed where the CNT act as the shish and induce growth of polymer (i.e., PE or nylon) crystal lamellae (kebabs), which periodically pattern the CNT.[7,30] In studies where PE/CNT hybrid crystals were grown

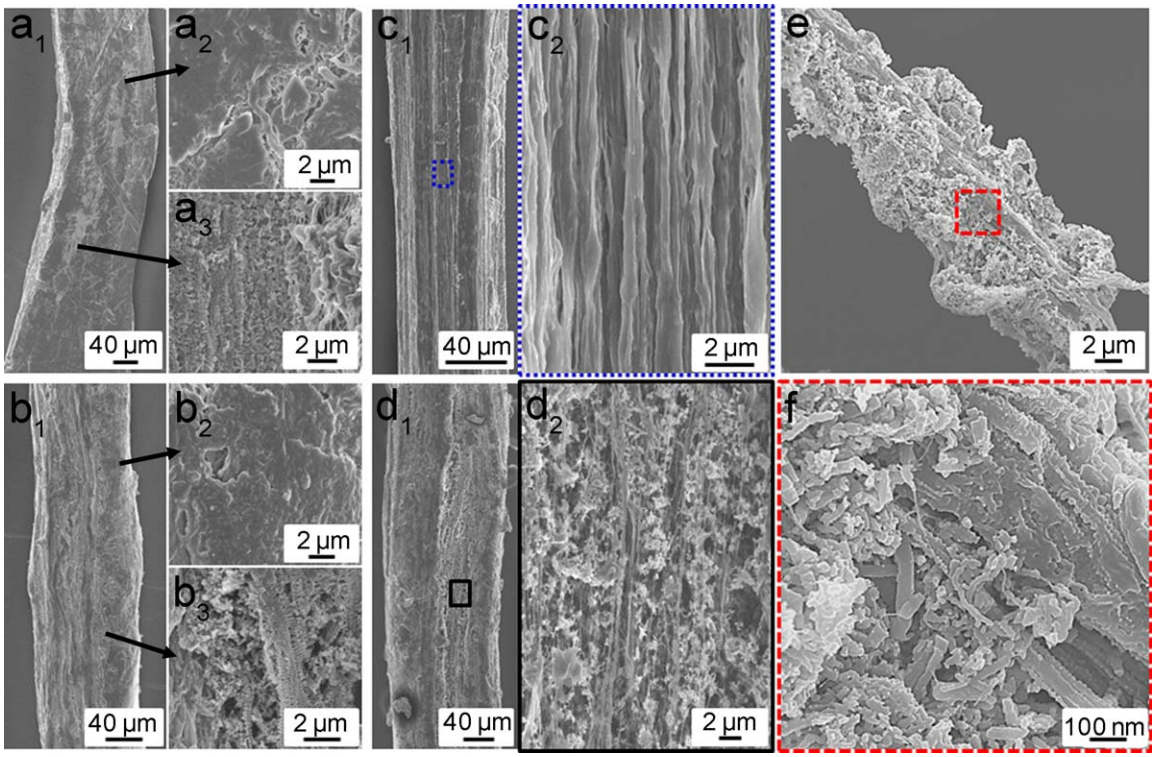

Figure 1. Scanning electron microscopy images of the PE and PE/CNCF fibrillar structures: (a_1) as-spun PE fiber (a_2) excess PE coating the fiber surface, (a_3) crack in the coating showing fibrils, (b_1) PE/CNCF as-spun fiber, (b_2) and (b_3) show coated and cracked surfaces of (b_1), (c_1) low, and (c_2) high-magnification images of drawn PE fiber showing fibrillar structure, (d_1) low and (d_2) high-magnification images of drawn PE/CNCF fiber showing fibrillar structure, (e) PE/CNCF fibrillar bundle showing a crust of CNCF surrounding PE fibrillar crystals (f) high magnification of the boxed region in (e) also showing the PE-rich and CNCF-rich regions. Arrows indicate the direction of the fiber axis. [Color figure can be viewed in the online issue, which is available at wileyonlinelibrary.com.]

under shear-flow, an additional ordered or extended-chain layer of PE is templated by the CNT, and the PE chains are oriented in the fiber direction.[5,6] These unique nucleating and templating abilities of CNT may be exploited through crystallization in order to achieve specific polymer morphological structures. Up to now, mostly low concentration CNT-polymer systems have been primarily studied. Relatively new work has begun to focus on other nanofiller systems including graphene nanoplatelets[31] and graphene nanochips.[26] In general, higher concentration nanofiller/polymer systems have been shown to retard crystallization.[31,32] Comparatively, low concentration polymer/carbon nanochip fibers have been shown to enable polymer crystallization and chain alignment through a sliding mechanism.[26]

In this work, shear crystallization of PE in the presence of carbon nanochip fibers (CNCF) will be investigated. The effect of CNCF on PE crystallization under shear flow and hot-drawing will be investigated in order to understand the crystal structure created and how the CNCF sliding mechanism can promote PE chain alignment and orientation. In terms of producing polymer nanocomposite fibers with high-mechanical properties along the axial direction, understanding how to form extended-chain crystal structure is key.[33] High performance fibers with extended-chain morphology are limited to only a few systems, for rod-like polymers[34] and PE.[35,36] As mentioned, several studies have highlighted the ability of various nanocarbons to template polymer crystal growth. This study is aimed at understanding the mechanism for using nanocarbons to promote extended-chain polymer crystal growth.

EXPERIMENTAL

Materials

All reagents were used without further purification. Xylenes (Certified ACS) and ultra-high molecular weight polyethylene (UHMWPE) ($\overline{M_w}$ 3,000,000–6,000,000 g/mol) were purchased from Sigma-Aldrich. Carbon Nanochip Fibers (CNCF) (purity >99 wt % C; batch H700) were purchased from Catalytic Materials.

Sample Characterization

Scanning electron microscopy (SEM) images were taken on a Zeiss Supra 25 Field Scanning SEM (operation voltage 5 kV). Samples were coated with chromium for imaging. Wide-Angle X-ray diffraction (WAXD) data was obtained using a Rigaku RAPID II curved detector system with a 3 kW sealed tube source (operating voltage 40 kV, current 30 mA, wavelength 0.1541 nm). WAXD data was analyzed using PDXL software from Rigaku and curve fitting for crystallinity measurements was performed in Origin 6.1. Small-Angle X-ray scattering (SAXS) diffraction was performed on a Rigaku MicroMax-007HF system with CuK_α radiation (operation voltage 40 kV and current 30 mA). Differential scanning calorimetry (DSC) was performed on a Q200 differential scanning calorimeter

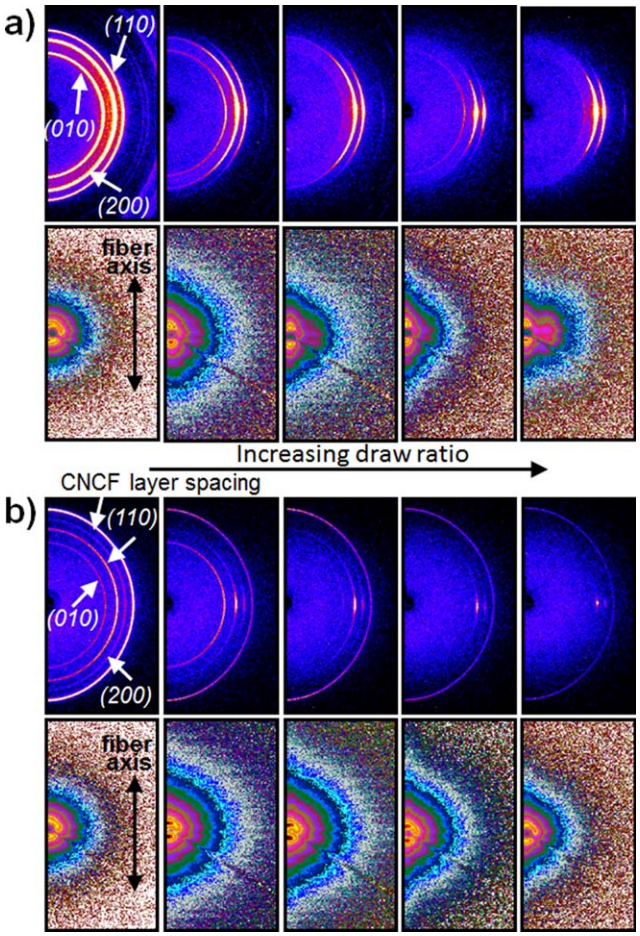

Figure 2. Diffraction patterns from both wide-angle X-ray diffraction (upper block) and small-angle X-ray scattering (lower block) for (a) control polyethylene and (b) hybrid polyethylene/CNCF fibrillar structures as a function of draw ratio. The draw ratio increases from 0 to 3 from left to right. [Color figure can be viewed in the online issue, which is available at wileyonlinelibrary.com.]

(manufactured by TA instruments). The heating rate was 10°C/min from room temperature (25°C) to 250°C. DSC data pertaining to the 1st heating curves is provided for all drawn PE and PE/CNCF fibers. The thermal history for fibers used in both DSC and X-ray diffraction/scattering analysis is the same. Tensile tests for the fibers were done using a RSA-G2 analyzer (TA Instruments). The sample gauge length was 10 mm and the strain rate was 0.02 mm/s. Thermogravimetric analysis (TGA) was performed in air using a Q50 thermogravimetric analyzer (manufactured by TA instruments). For TGA measurements samples were heated from room temperature (25°C) to 800°C at a heating rate of 10°C/min.

Fabrication of PE/CNCF Fibrillar Crystals

Xylenes were used to both dissolve PE and disperse CNCF. CNCF are nanofibers, which consist of flattened stacked few-wall nanotubes. These flattened nanotubes are able to slide with respect to one another during sonication, mixing, as well as the fiber spinning processes. The morphological features of these CNCF has been discussed and illustrated in detail previously by the authors.[26] PE was dissolved in xylenes between 130 and 140°C at a concentration of 0.02 wt %. CNCF were sonicated in xylenes at a concentration of 1.7 mg/mL in a bath sonicator (Fisher FS30 bath sonicator, frequency 43 kHz, power 50 W) for 24 h at ~55°C. Fibrillar crystallization (i.e., the formation of extended-chain crystals with growth front along the chain axis) was performed in several steps. To form control PE fibrillar crystals, the dilute PE solution is subjected to shear flow. The shear flow is created using a concentric cylinder set-up, which was previously used in other work by the authors.[5] The stir rod is composed of a shaft fitted with a cylindrical stirrer comprised of Teflon. An overhead mechanical stirrer (Eurostar power-b IKA® WERKE stirrer) is used to produce a rotation speed of 800 rpm. After the PE is fully dissolved at the dissolution temperature, the solution temperature is reduced to the crystallization temperature of ~90°C. The flow is maintained constant during crystal formation. The fibrillar crystals were subsequently collected on the Teflon cylindrical stirrer. The crystals are removed from the stirrer after the PE solution is cooled to room temperature (25°C). During cooling the PE fibrillar crystals are coated with excess PE still present in the solution. This coating phenomenon is well known to occur after the formation of PE fibrillar crystal structures.[5,17] A subsequent washing step can be used to reveal the PE fibrillar structure. The fibrillar crystals are also known to form bundles or macro-fibers.[17]

To form the hybrid PE/CNCF fibrillar crystals and subsequent macro-fibers, CNCF is injected into the dilute PE solution under shear flow at the onset of the PE crystallization temperature (i.e., ~90°C). Before injection of the CNCF, the dispersion was resonicated for ~5 to 10 min to ensure uniform dispersion. A glass syringe with a 26-gauge blunt tip needle was used to inject 1 mL of CNCF dispersion into the PE solution in order to achieve a final weight concentration of 25 wt % CNCF to PE solid content in the solution. All fibrillar crystals in the form of macro-fibers were removed for subsequent analysis and no washing step was used. Hot-drawing of the fibers was performed on a hot plate maintained at 130°C. The unwashed as-spun fibers were drawn between 1.5 and 3 times their original length.

RESULTS AND DISCUSSION

PE control and PE/CNCF fibrillar crystals were fabricated using the shear flow set-up outlined in the experimental section. Both control and composite resultant macro-fibers consist of bundled fibrillar crystals, which exhibit a shish-kebab structure (Figure 1). Each macro-fiber (i.e., diameter ~80–100 μm before hot drawing) consists of bundles of fibrillar crystals ranging in diameter from 25 to 200 nm. This characteristic shish-kebab (SK) structure has been observed previously for PE and PE composite fibrils grown under shear.[5,12,37] In this work, the presence of the SK structure is not very obvious on the surface of the as-spun PE and PE/CNCF fibers due to excess (i.e., nonfibrillar) PE coating [Figure 1(a,b)]. This coating occurs once the shear crystallization experiment is halted (i.e., stopping the rotation of the stir bar) to remove the fibers for observation. Before removing the macro-fibers from the stir bar, the PE fibers are cooled to room temperature (25°C), and for this reason excess PE in the solution can

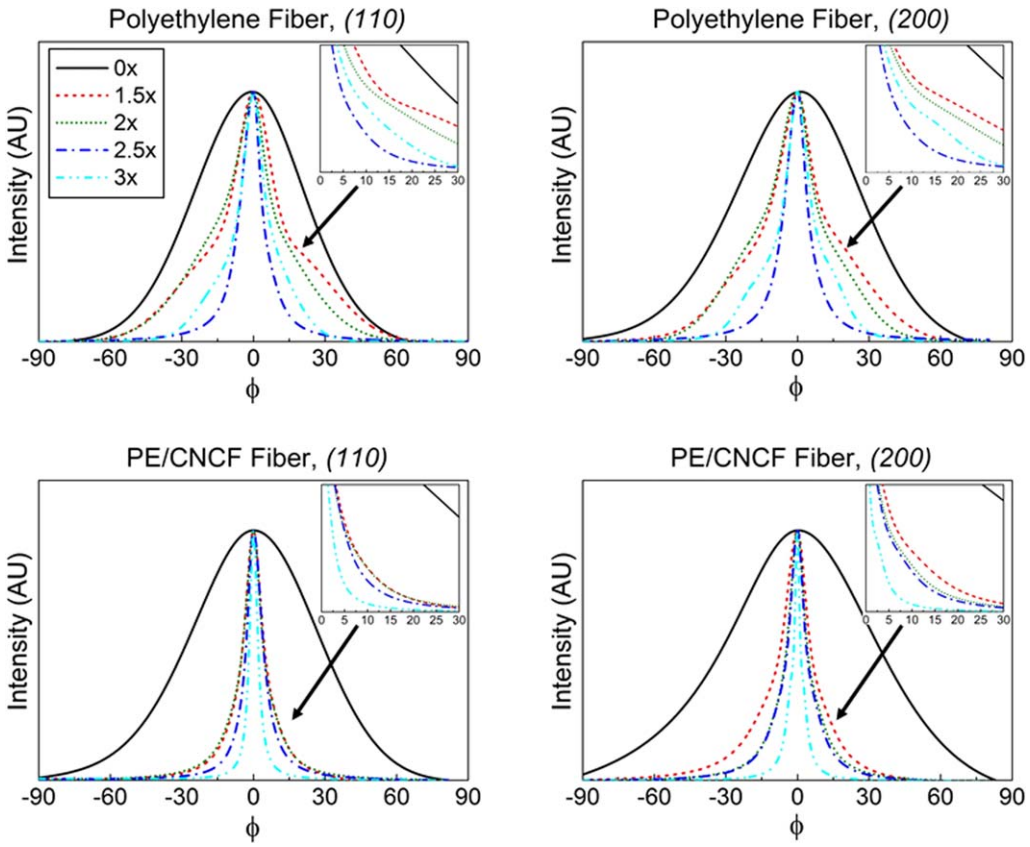

Figure 3. Wide-angle X-ray diffraction azimuthal intensity scans of control polyethylene (top row) and composite polyethylene/CNCF (bottom row) fibers at each drawing stage for both the predominant (*110*) (left column) and (*200*) (right column) reflections. A distinct shoulder in the azimuthal scans is observed as drawing increases. Each inset shows a magnified view of the azimuthal curves between 0° and 30° where this shoulder can be clearly observed. [Color figure can be viewed in the online issue, which is available at wileyonlinelibrary.com.]

form a thin coating on the fibers. As mentioned, a subsequent washing step may be performed to remove the excess PE coating and reveal the fibrillar structure. However, washing was not performed in this work since this process compromises the mechanical integrity of the fiber and as a result the as-spun fibers cannot be hot-drawn. For both fiber samples, the bundle of fibrillar crystals and SK structure can be observed at cracked regions in the fiber surface [Figure 1($a3_3$,$b3_3$)]. As expected, an increase in overall fibrillar alignment occurs during hot-drawing [Figure 1(c,d)]. For both PE and PE/CNCF fibers, the fibrillar bundles visually become much more aligned post hot-drawing [Figure 1($c2_2$,$d2_2$)]. This change in PE chain orientation as a function of drawing is quantified using WAXD analysis.

As mentioned in the experimental section, in order to form the PE/CNCF hybrid crystals a CNCF dispersion was injected into the sheared PE solution at the crystallization temperature of ~90°C. In this study the solid CNCF concentration was ~25 wt % with respect to the PE. The injection speed of the CNCF dispersion was controlled at ~0.25 mL/min. It has been estimated in previous work that the growth rate of the PE crystals formation under shear ranges from 2 to 40 cm/min.[17] Similar fibrillar crystallization conditions are used in this work, therefore, a comparable growth rate is assumed. Because of the potential mismatch between the growth rate of the PE crystal and injection rate of the CNCF into the solution, in some cases the CNCF are only partially incorporated into the fibrillar crystals,[17] while the remaining CNCF adhered to the surface of the hybrid fibrillar structure. TGA was used to examine the concentration of CNCF in the composite fibers based on degradation behavior. The onset of PE degradation was observed at ~225°C and rapid weight lost occurred after ~285°C. It was also found that for the PE used in this work, complete charring occurred at ~465°C. The onset of CNCF degradation occurred at ~548°C with rapid loss beginning at ~595°C, and complete charring at ~700°C. Using this TGA analysis the overall residual CNCF content (i.e., material exhibiting degradation at >550°C) was found to range from 19 to 25 wt % for the various composite samples. For this reason, the weight content of CNCF incorporated into the composite fibers is considered to be a significant portion of the original amount added to the crystallizing solution for fibrillar formation.

Under the aforementioned spinning approach, typically a crusted fiber structure is observed for the PE/CNCF hybrids [Figure 1(e)]. The crust is a CNCF-rich region intermingled with only a small amount of polymer [Figure 1(f)]. It was found that the crystallization temperature at which the CNCF are introduced and the CNCF injection rate played a significant role on the overall final structure of the PE/CNCF fibrillar crystal morphology. If the solution temperature was too high (>90°C) upon injection, no crystals formed and the CNCF

Table I. Listing of Wilchinsky's Method Parameters as well as Herman's Orientation Values (f) for Both Control and CNCF Composite Polyethylene Fibers at Different Draw Ratios

	Wilchinsky's method parameters and Herman's orientation values											
	Polyethylene fiber ($\rho_{110} = 56.3°$, $\rho_{200} = 0°$)					CNCF composite fiber ($\rho_{110} = 56.3°$, $\rho_{200} = 0°$)						
Draw ratio	$Cos^2\phi_{110,\ avg}$	$\cos^2\phi_{200,\ avg}$	$\cos^2\theta_{c,avg}$	$f_{b,\ avg}$	$f_{b,\ kebab}$	$f_{b,\ shish}$	$\cos^2\phi_{110,\ avg}$	$\cos^2\phi_{200,\ avg}$	$\cos^2\theta_{c,\ avg}$	$f_{b,\ avg}$	$f_{b,\ kebab}$	$f_{b,\ shish}$
0	0.193	0.293	0.558	0.337	0.002	0.518	0.172	0.196	0.643	0.465	0.365	0.539
1.5	0.156	0.160	0.685	0.528	0.453	0.820	0.079	0.089	0.837	0.755	0.716	0.885
2	0.130	0.133	0.739	0.608	0.543	0.837	0.065	0.069	0.867	0.801	0.747	0.913
2.5	0.066	0.086	0.857	0.786	0.610	0.913	0.052	0.058	0.892	0.839	0.797	0.936
3	0.082	0.096	0.828	0.742	0.737	0.883	0.050	0.052	0.898	0.847	0.835	0.931

f values are also calculated for the shish (i.e., narrow) and kebab (i.e., broad) orientation populations observed in the fibers (see Figure 4a and 4b).

formed large aggregates immediately upon injection. On the other hand, if the solution temperature was too low, PE crystals formed prior to CNCF being injected causing the PE crystals to be CNCF deficient. Therefore, in this work an in depth analyses of only the 90°C formed PE/CNCF macrofibers are discussed as they compare to the control PE samples.

For the as-spun fibers three major wide-angle X-ray reflections (*110*), (*200*), and (*010*) are observed, and each are inherent to the PE orthorhombic [(*110*) and (*200*) reflections] and triclinic [(*110*) reflection] crystal structures [Figure 2(a)].[20] For the composite fibers, an additional diffraction ring representing the CNCF layer spacing *(002)* is also observed [Figure 2(b)]. Wide-angle X-ray patterns show that for both the control and composite fibers as the draw ratio increases from 1.5 to 3 the polymer chain orientation also improves (Figure 2). The CNCF orientation [i.e., (*002*) peak] does not show any obvious orientation changes owing to its inherent layered platelet structure.[26] PE chain orientation factor values (f) with respect to the fiber axis for each fibrillar structure were calculated using both the (*110*) and (*200*) reflection peaks by Wilchinsky's method[38] (Table I). An orientation factor of $f = 1$ would represent fully oriented PE fibrils along the fiber axis, while an orientation factor of 0 represents fibrils randomly aligned along the fiber axis. Subsequently, fibrils aligned perpendicular to the fiber axis would have an orientation factor of -0.5. The parameters used for the orientation calculations are also provided in Table I, where ρ_{hkl} is the angle between the plane normal and *c*-axis of the PE unit cell, $\overline{\cos^2\phi_{hkl}}$ is the orientation of each (*hkl*) plane determined from the X-ray azimuthal data using Wilchinsky's equation, and $\overline{\cos^2\theta_c}$ is the overall orientation of the polymer chain with respect to the fiber axis used to determine the orientation factor.

On the basis of these WAXD results, composite fibers show higher degrees of orientation for both as-spun and drawn fibers as compared to the control samples (Table I). Composite fibers drawn three times have a maximum overall average orientation value of 0.847, while for the control fibers it is only 0.786 (note: draw ratio for maximum orientation in the control fiber is 2.5 times). Greater orientation for the PE/CNCF hybrid fibrillar structures is attributed to both the sliding effect or lubricating ability of the CNCF[26] and the ability of the nanocarbon to template polymer orientation and alignment.[6,39]

Further analysis of the WAXD azimuthal curves for the (*110*) and (*200*) PE peaks indicate that the overall orientation of the polymer chains represent two distinct populations. The raw azimuthal curves for the fibers as a function of draw ratio are shown in Figure 3. The azimuthal curves are fitted by two curves [Figure 4(a,b)]. The broader peak represents more disordered PE associated with kebab orientation, while the narrow peak is representative of more ordered chains consistent with shish orientation. As the draw ratio increases the shoulder in the azimuthal curves begins to diminish, which is consistent with the increase in the overall chain orientation. During drawing there is a pullout or unfolding of PE chains from the kebabs (folded-chain) into shish (extended-chain) structures as the

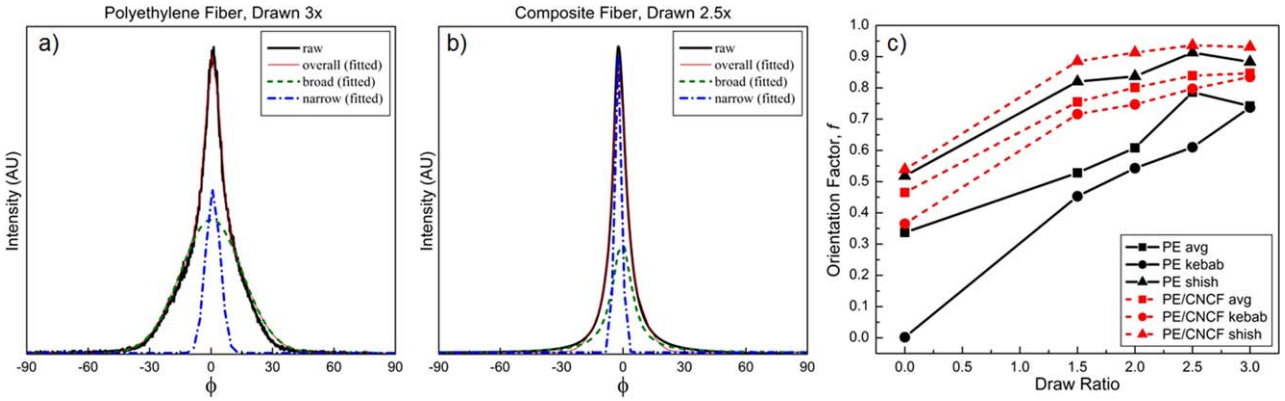

Figure 4. Wide-angle X-ray diffraction azimuthal intensity scans for the (*110*) reflection and their corresponding fitting for both populations of PE orientation (associated with the shish (i.e., narrow) and kebab (i.e., broad) structures): (a) control PE-drawn 3×, (b) PE/CNCF-drawn 2.5×. (c) Graph showing the change in orientation factor as a function of drawing ratio for both PE and PE/CNCF fibrillar structures. The average orientation factors as well as those associated with the kebab and shish crystal population are also shown. [Color figure can be viewed in the online issue, which is available at wileyonlinelibrary.com.]

alignment increases/improves. The hybrid PE/CNCF fibers in general show narrower intensity peaks indicating higher orientation than the control fibers. In addition, the curves for the PE/CNCF fibers show a less pronounced shoulder before drawing indicating that the orientation of the kebabs and shish crystals are more closely related. As mentioned, the calculated average orientation values as well as those associated with the kebab and shish crystal growth are all listed in Table I. It was found that regardless of the draw ratio, PE/CNCF fibers always showed greater overall orientation values as compared to the control fibers [Figure 4(c)].

In addition to WAXD, SAXS measurements were also used to look at the long-range order and morphological structure of the PE and PE/CNCF fibers. The SAXS patterns for both sets of samples are shown in Figure 2(a,b). It is clear that an equatorial streak consistent with shish crystal growth[10,40] becomes more pronounced as the draw ratio increases for the fibers. Simultaneously, a meridional lobe consistent with kebab/lamellar development[10] is also observed. However, this is only obvious in the control fibers. These results show that as the draw ratio increases, more extended-chain crystals are formed. As compared to the control, the hybrid fibers exhibit a much more pronounced equatorial steak indicating a larger population of extended-chain crystals. The control fibers show a well-defined meridional lobe, and the lamellar thickness calculated from SAXS is ~48 nm [Figure 5(a)]. Meridional lobes are less pronounced and more diffused in the PE/CNCF samples. The SAXS peak intensity profiles for both samples show that development of the meridional intensity is more obvious for the control PE as compared to the PE/CNCF fibers [Figure 5(b)]. These weak and undefined meridional lobes associated with the PE/CNCF crystals illustrate that kebab development is very inconsistent in these samples. This may also indicate that the CNCF play a role in disrupting the development of regular kebab periodicity during shear crystallization and subsequent drawing. In terms of the control samples, the kebab growth is more uniform. However, the large lamellar thickness and diffused scattering of the meridional lobe suggests a loose kebab structure.

To further compare shish versus kebab growth, the Halo method[41] was used to determine the change in SAXS intensity along the equatorial and meridional directions [Figure 5(c,d)]. Azimuthal scans were taken as a function of φ, for each pattern, and plotted against q (the diffraction vector $q=4\pi/\lambda sin\theta$, where λ is the wavelength of the X-ray beam and θ is the Bragg angle at which the scattering peak is observed). The azimuthal intensities for the undrawn samples were used as baseline measurements for the initial existence of the kebab and shish in the as-prepared fibers. The changes in equatorial and meridional intensities were determined by subtracting the SAXS azimuthal intensity profiles of each sample at increasing draw ratio from the baseline intensity. On the basis of this analysis, it is shown that up to about a draw ratio of two, the shish and kebab crystals grow at a relatively even rate [Figure 5(c,d)]. At this point there is a change where the shish growth becomes more dominant in both samples as the draw ratio is further increased to 2.5 times. Upon further drawing, for the control fibers the shish growth reaches a plateau and kebab growth becomes most dominant. This may be related to the self-seeding of PE kebab growth on shish in the SK structure.[42] On the other hand for the PE/CNCF fibers, shish growth continues to be most predominant indicating that the presence of the nanocarbon helps to promote extended-chain formation.

In addition to the orientation calculations, the WAXD data also shows that both PE and PE/CNCF fibers produced are highly crystalline. Both crystallinity of the fibers and crystal size for each (*hkl*) peak were measured. Figure 6(a) shows the typical fitted WAXD curves for both PE and PE/CNCF fibers to obtain the overall percent crystallinity (X_{WAXD}). It is observed that the crystallinity for the both sets of fiber samples is very high (Table II), and this is expected since both the control and PE/CNCF fibers are grown using shear crystallization procedures.[37] There is also no significant change in the overall crystallinity as a function of drawing. In general the PE/CNCF fibers exhibit a slightly lower overall percent crystallinity as compared to the control samples. This lower composite crystallinity is thought to be due to some retardation of polymer crystallization due to the injection of

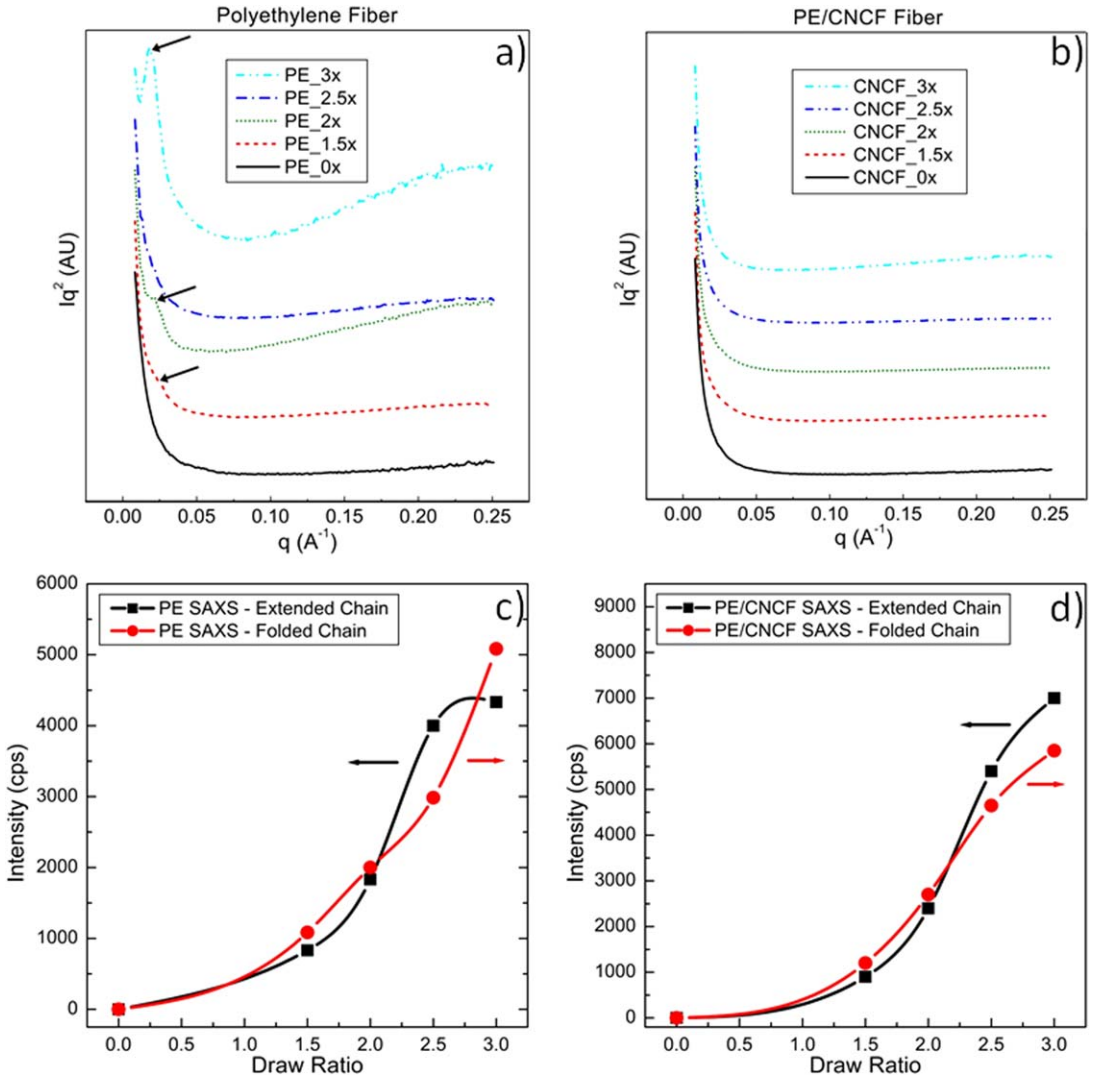

Figure 5. (a, b) Small-angle X-ray scattering intensity profiles for (a) PE and (b) PE/CNCF fibers. Iq^2 as a function of $q(q=4\pi/\lambda sin\theta)$ shows the development of the meridional intensity (kebabs) for the control polyethylene fibrillar crystals. (c, d) Plots of the small-angle scattering intensity along the equatorial (i.e., extended-chain) and meridional (i.e., folded-chain) directions as a function of draw ratio for both the control (c) and hybrid PE/CNCF (d) fibers showing an increase in extended-chain crystal growth at draw ratios over two. [Color figure can be viewed in the online issue, which is available at wileyonlinelibrary.com.]

undispersed CNCF, which has been previously observed.[43] PE crystal sizes for both as-spun and drawn control and hybrid fibers are also provided in Table II. For both fibers, the crystal size remains similar as the draw ratio increases. The fibers are drawn near the melting temperature at 130°C, therefore, it is expected that rearrangement of the polymer chains during drawing will cause slight variations in the crystal size. The weaker (*010*) peak, which is associated with a PE triclinic phase/modification[17] diminishes as the drawing increases. In this study, to increase the draw ratio the fibers drawn are exposed to the hot plate (at 130°C) for longer duration times. The presence of the triclinic phase is indicated by the (*010*) peak and is known to disappear around 130°C.[37] Therefore, the diminishment of this peak becomes more pronounced at higher draw ratios.

Thermal analysis using DSC was also performed on both the PE and PE/CNCF fiber samples. DSC analysis of the as-received PE powders shows a single melting endotherm for the unconstrained crystals. For the PE and PE/CNCF fibers the melting endotherms observed are associated with melting of the unconstrained PE crystals [Figure 6(b,c)]. It should be noted that the samples for both WAXD and DSC analysis are the same. As mentioned, only the 1st heating curve is analyzed for DSC, to ensure that the data is comparable in terms of the thermal history of the fiber samples. The percent crystallinity (X_{DSC}) determined using the enthalpy of melting (ΔH_m) from the DSC analysis is significantly lower than the values from WAXD. In addition, it is observed that the overall enthalpy of melting for the PE/CNCF fibers is much lower as compared to the control fibers (Table II). The reason for the disparity between X_{WAXD} and X_{DSC} is related to the confinement of the PE crystals due to the fibrillar formation and restriction as a result of the presence of the CNCF. Confinement of the PE crystal leads to incomplete melting of the crystals, which is reflected in the 1st heating

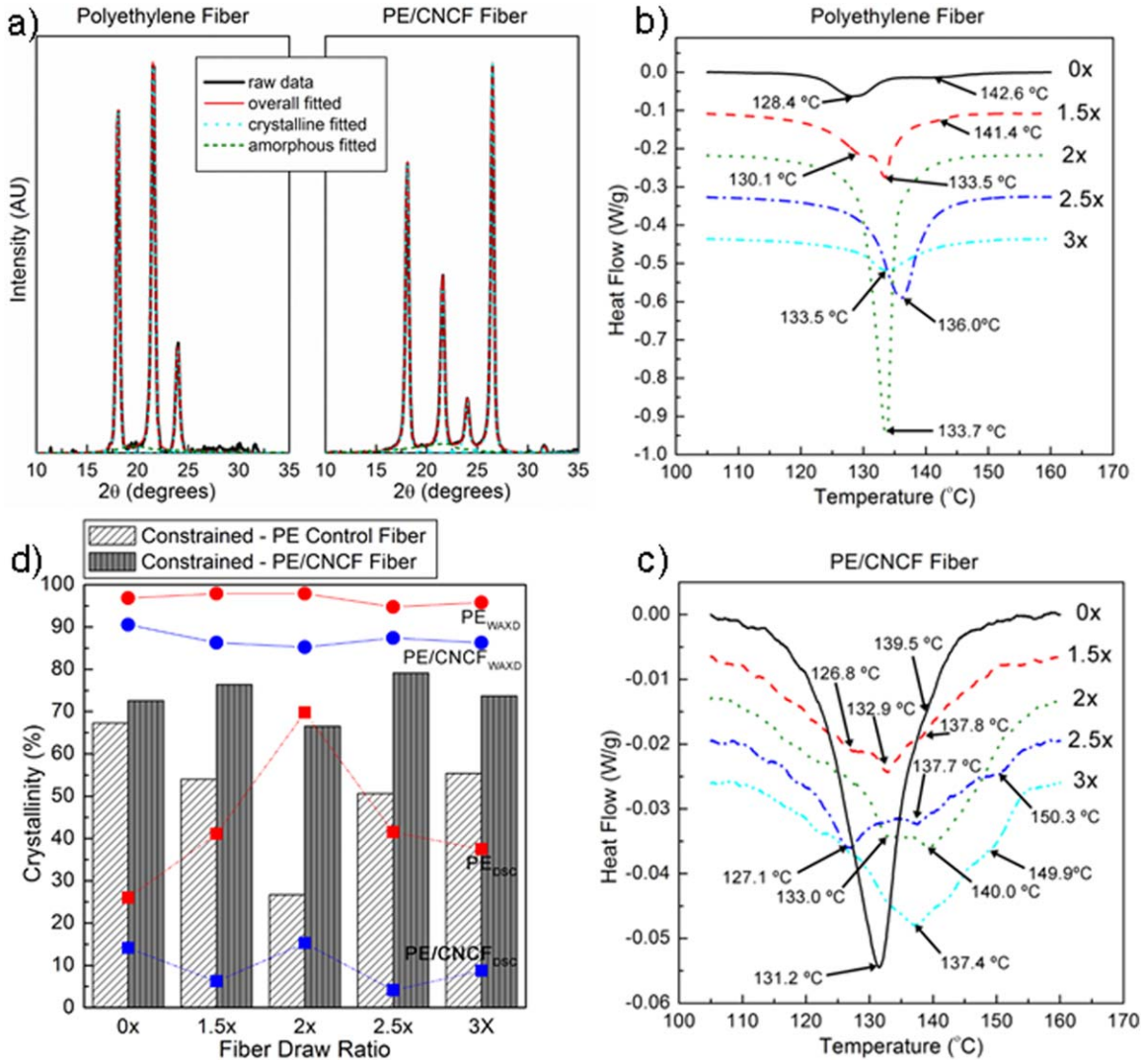

Figure 6. (a) WAXD intensity profiles fitted to show crystalline and amorphous regions of the PE fibrillar structure. (b, c) Differential scanning calorimetry curves showing the melting transition for both control PE (b) and hybrid PE/CNCF (c) fibers at each draw ratio. (d) Graphical comparison of the overall, constrained, and unconstrained fiber crystallinity calculated from WAXD and DSC measurements. [Color figure can be viewed in the online issue, which is available at wileyonlinelibrary.com.]

curves. Comparing the ΔH_m from the control fibers to the composites provides evidence that the interaction between the CNCF and PE in the hybrid fibrillar crystals results in more confinement of the polymer chains. Figure 6(d) compares the crystallinity (X) values obtained from both WAXD and DSC and also shows the percent of constrained crystals for the control and composite. The trend shows that the constrained crystal content is much higher in the composite as compared to the control fibers.

For the control PE samples, there is a larger percentage of unconstrained fibrillar crystals (i.e., higher ΔH_m). However, there is a noticeable shift in the melting temperature for the unconstrained fibrillar crystals as a function of drawing. This is due to the increase of order/alignment in the crystals as evidenced by both WAXD and SAXS studies discussed earlier. Figure 6(d) also shows that the constrained crystal content first decreases then increases with draw ratio. During the hot-drawing process the fibers are exposed to the hot plate at 130°C. In other words, the higher draw ratios correspond to a longer duration time on the hot-plate. Therefore, remelting and reformation of the PE crystals occur during this time. However, as chain alignment increases, the PE crystals become more confined and the constrained percentage again increases.

For PE/CNCF samples a new melting peak at ~150°C, is also observed post drawing (i.e., draw ratio 2.5 and 3) [Figure 6(b,c)], and this is not found in the control fiber samples. This high order peak is attributed to a transformation of the orthorhombic PE to a hexagonal lattice.[19] This transition is often observed in constrained fibrillar crystal samples.[19] These hexagonally packed crystals are known to be the most ordered PE crystals and consist of chains in the extended conformation. The evidence of this peak in the hybrid PE/CNCF structures suggests that the presence of CNCF can aid in inducing this most ordered crystal structure growth. Prior work has also

shown the ability of these unique nanocarbons to act as lubricating agents to facilitate polymer chain extension.[26] During drawing the CNCF are able to template highly ordered extended-chain PE. This increase in chain order and templating may also contribute to total content of constrained crystals [Figure 6(d)] as well as only small variation in its content as a function of drawing.

Some preliminary mechanical analysis shows that the fiber strength improves significantly with increased drawing. After a maximum draw ratio of three, the PE fibrillar structures increased in tensile strength by 231%, while PE/CNCF fibrils increased by 435% as compared to the undrawn samples. A similar trend in the tensile modulus is also observed (i.e., 457% for PE and 1155% for PE/CNCF fibrillar structures). This large increase in strength and modulus further supports the evidence showing an overall increase in orientation for the fibrillar structures during drawing. In addition, the overall modulus increase for the PE/CNCF hybrid is much more pronounced than that for the PE fibers, and this may be due to the large degree of orientation and population of shish crystals as compared to the drawn control structures.

It is also interesting to note that the best mechanical performance for each sample set (i.e., control and composite) occurs at a draw ratio of two (Figure 7). At this draw ratio the SAXS data shows that both kebab and shish crystal growth is very similar in each of the fibers [Figure 5(c,d)]. This may contribute to a more uniform fibrillar morphology and subsequent macrofiber structure in each fiber. Comparing both the control and composite fiber at draw ratio 2, it is found that the PE/CNCF samples exhibit lower average mechanical properties as compared to the control fibers. The presence of CNCF aggregates in the composite fibers, which act as defects, may contribute to the lower average values as well as the fluctuation in the properties measured as compared to the control (Figure 7).

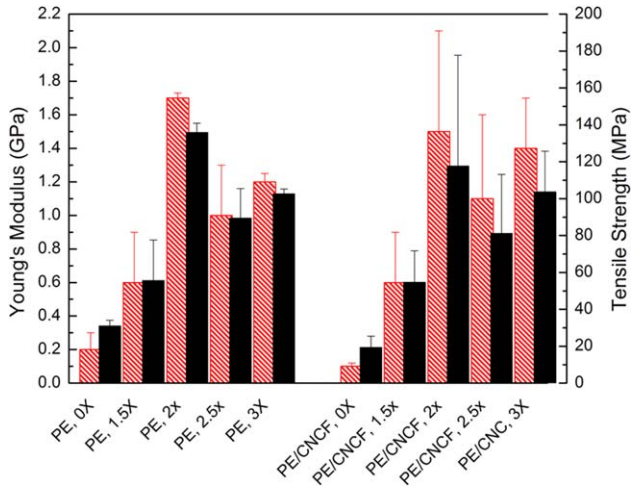

Figure 7. Young's modulus (red-dashed) and tensile strength (black-solid) of control PE and hybrid PE/CNCF fibers plotted as a function of the draw ratio. The modulus and tensile strength increases by 457% and 231% for the control and 1155% and 435% for the hybrid at a draw ratio of three, respectively. [Color figure can be viewed in the online issue, which is available at wileyonlinelibrary.com.]

Table II. Listing of the Crystal Size for the Major *(010)*, *(110)*, and *(200)* Reflections as well as the Crystallinity Measured from Wide-Angle X-ray Diffraction

	Polyethylene fiber						PE/CNCF composite fiber					
	Crystal size, L_{hkl} (nm)			$X_{overall}$ (%)[a]	$\Delta H_{m,\ DSC}$ (J/g)	$X_{unconstrained}$ (%)[b]	Crystal size, L_{hkl} (nm)			$X_{overall}$ (%)[a]	$\Delta H_{m,\ DSC}$ (J/g)	$X_{unconstrained}$ (%)[b]
Draw ratio	$(010)_{triclinic}$	*(110)*	*(200)*	WAXD		DSC	$(010)_{triclinic}$	*(110)*	*(200)*	WAXD		DSC
0	23	19	16	97	87.0	30	25	22	17	91	54.7	19
1.5	12	21	18	98	129.1	44	26	20	17	87	32.3	11
2	21	21	18	98	209.0	71	23	20	16	86	57.0	19
2.5	17	20	17	95	130.3	44	—	17	17	88	26.7	9
3	—	21	18	96	119.1	41	17	16	17	87	39.2	13

The enthalpy of melting determined from differential scanning calorimetry is also listed for as-spun and drawn control PE and PE/CNCF composite fibers.
[a] The crystalline percentage is measured from WAXD and represents the overall crystal content in the fibers.
[b] The crystalline percentage is calculated from the enthalpy of melting (ΔH_m) measured using the 1st DSC melting curve. This crystal percent represents only the unconstrained crystals present in the fibers.

The overall mechanical properties for the fibers in this work are fairly low as compared to high-strength composite fibers currently being manufactured today (e.g., Spectra®[35] and Dyneema®[36]), and this may be due to the presence of many voids in the macrofibers due to the bundling of the fibrillar crystals (Figure 1) to form the macrofibers. These voids greatly diminish the mechanical properties of the macrofibers, as both decreased load transfer and imperfections considerably reduce overall fiber strength.

Initial studies on PE shish-kebab crystal growth under shear, has shown that it is possible to grow highly ordered (i.e., shish) polymer phases. However, this work shows direct evidence of the ability to use nanocarbons as a template for highly ordered polymer phase formation in hybrid materials. This study also provides the evidence that the rigidity, size, and sliding mechanism of the nanocarbon within the polymer matrix can play a significant role in the formation of a specific type of polymer architecture. These fundamental studies provide insight toward developing processing methods to use nanocarbon fillers as templating materials as well as reinforcements in polymer matrices.

CONCLUSIONS

It is important to understand polymer crystallization in order to comprehend and control polymer structures and their resultant properties. In this study PE/CNCF composite fibers were fabricated under shear flow. Subsequent hot drawing took place to further align and orient the polymer chains. The unique interactions between PE and CNCF through crystallization under shear yielded composite fibers in which hybrid shish-kebab PE/CNCF crystals were formed. The presence of CNCF was determined through WAXD analysis to increase the orientation of the polymer chains. SAXS analysis also showed extended-chain crystallization was more pronounced in the presence of CNCF. In addition, DSC supported the SAXS evidence of extended-chain crystal structure, and showed that these highly ordered PE crystals are confined by the CNCF. This work adds to the literature which shows the ability for nanocarbons to template extended-chain polymer structures in a composite. These fundamental scientific understandings provide insight into the underpinnings that affect tailoring specific polymer morphology and properties for various nanocarbon/polymer composite applications.

ACKNOWLEDGMENTS

The authors would like to acknowledge the basic research support from the Air Force Office of Scientific Research (AFOSR) (FA9550-11-1-0153). WAXD and SAXS instrumentation in the MINUS lab was funded through the Defense University Research Instrumentation Program (DURIP) within the Department of Defense (DoD).

REFERENCES

1. Pang, H.; Zhong, G. J.; Xu, J. Z.; Yan, D. X.; Ji, X.; Li, Z. M.; Chen, C. *Chin. J. Polym. Sci.* **2012**, *30*, 879.
2. Wu, J. H.; Yen, M. S.; Chen, C. W.; Kuo, M. C.; Tsai, F. K.; Kuo, J. S.; Yang, L. H.; Huang, J. C. *J. Appl. Polym. Sci.* **2012**, *125*, 494.
3. Pang, H.; Zhong, G. J.; Wang, Y.; Xu, J. Z.; Li, Z. M.; Lei, J.; Chen, C.; Ji, X. *J. Polym. Res.* **2012**, *19*, 9837.
4. Ahangari, M. G.; Fereidoon, A.; Kordani, N.; Garmabi, H. *Polym. Bull.* **2011**, *66*, 239.
5. Minus, M. L.; Chae, H. G.; Kumar, S. *ACS Appl. Mater. Interfaces* **2012**, *4*, 326.
6. Minus, M. L.; Chea, H. G.; Kumar, S. *Polymer* **2006**, *47*, 3705.
7. Li, C. Y.; Li, L. Y.; Cai, W. W.; Kodjie, S. L.; Tenneti, K. K. *Adv. Mater.* **2005**, *17*, 1198.
8. Haggenmueller, R.; Fischer, J. E.; Winey, K. I. *Macromolecules* **2006**, *39*, 2964.
9. Lieberwirth, I.; Loos, J.; Petermann, J.; Keller, A. *J. Polym. Sci. Part B: Polym. Phys.* **2000**, *38*, 1183.
10. Somani, R. H.; Yang, L.; Zhu, L.; Hsiao, B. S. *Polym.* **2005**, *46*, 8587.
11. Pennings, A. J.; Kiel, A. M. *Colloid. Polym. Sci.* **1965**, *205*, 160.
12. Pennings, A. J.; van der Mark, J. M. A. A.; Kiel, A. M. *Colloid. Polym. Sci.* **1969**, *237*, 336.
13. Zwijnenburg, A.; Pennings, A. *J. Colloid Interface Sci.* **1975**, *253*, 452.
14. Tzavalas, S.; Drakonakis, V.; Mouzakis, D. E.; Fischer, D.; Gregoriou, V. G. *Macromolecules* **2006**, *39*, 9150.
15. Cadek, M.; Coleman, J. N.; Ryan, K. P. *Nano Lett.* **2004**, *4*, 353.
16. Li, L.; Li, B.; Hood, M. A.; Li, C. *Polymer* **2009**, *50*, 953.
17. Pennings, A. J. *Makromol. Chem. Suppl.* **1979**, *2*, 99.
18. Lemstra, P. J.; van Aerle, N. A. J. M.; Bastiaansen, C. W. M. *Polym. J.* **1987**, *19*, 85.
19. Smith, P.; Lemstra, P. J. *J. Mater. Sci.* **1980**, *15*, 505.
20. Zwijnenburg, A.; Van Hutten, P. F.; Pennings, A. J.; Chanzy, H. D. *Colloid. Polym. Sci.* **1978**, *256*, 729.
21. Kubi, H.; Okamoto, M.; Kotaka, T. *Polymer* **1998**, *39*, 4827.
22. Zwijnenburg, A.; Pennings, A. *J. Colloid Interface Sci.* **1976**, *254*, 868.
23. Baughman, R. H.; Zakhidov, A. A.; de Heer, W. A. *Science* **2002**, *297*, 787.
24. Dalton, A. B.; Collins, S.; Munoz, E.; Razal, J. M.; Ebron, V. H.; Ferraris, J. P.; Coleman, J. N.; Kim, B. G.; Baughman, R. H. *Nature* **2003**, *423*, 703.
25. Vega, J. F.; Martinez-Salazar, J.; Trujillo, M.; Arnal, M. L.; Muller, A. J.; Bredeau, S.; Dubois, P. *Macromolecules* **2009**, *42*, 4719.
26. Song, K.; Zhang, Y.; Meng, J.; Minus, M. L. *J. Appl. Polym. Sci.* **2012**, *127*, 2977.
27. Zhang, Y.; Song, K.; Meng, J.; Minus, M. L. *ACS Appl. Mater. Interfaces* **2013**, *5*, 807.
28. Meng, J.; Zhang, Y.; Song, K.; Minus, M. L. *Macromol. Mater. Eng.* **2014**, *299*, 144.
29. Zhang, S.; Lin, W.; Wong, C.-P.; Bucknall, D. G.; Kumar, S. *Appl. Mater. Interfaces* **2010**, *2*, 1642.

30. Li, L. Y.; Li, C. Y.; Ni, C. Y. *J. Am. Chem. Soc.* **2006**, *128*, 1692.

31. Jiang, X.; Drzal, L. T. *Polym. Compos.* **2012**, *33*, 636.

32. Di Maio, E.; Iannace, S.; Sorrentino, L.; Nicolais, L. *Polymer* **2004**, *45*, 8893.

33. Chae, H. G.; Kumar, S. *Science* **2008**, *319*, 908.

34. DuPont, http://www.dupont.com/.

35. Honeywell International, Inc. http://www.honeywell-advancedfibersandcomposites.com/.

36. DSM, http://www.dsm.com/corporate/about/business-entities/dsm-dyneema.html.

37. Pennings, A. J.; Zwijnenburg, A. *J. Polym. Sci. Part B: Polym. Phys.* **1979**, *17*, 1011.

38. Klug, H. P.; Alexander, L. E. X-Ray Diffraction Procedures For Polycrystalline and Amorphous Materials, 2nd ed.; Wiley: New York, **1954**.

39. Garcia-Gutierrez, M. C.; Nogales, A.; Rueda, D. R.; Domingo, C.; Garcia-Ramos, J. V.; Broza, G.; Roslaniec, Z.; Schulte, K.; Davies, R. J.; Ezquerra, T. A. *Polymer* **2006**, *47*, 341.

40. Camarillo, A. A.; Stribeck, N. *Fibres Text. East. Eur.* **2005**, *13*, 27.

41. Ran, S.; Zong, X.; Fang, D.; Hsiao, B. S.; Chu, B.; Ross, R. *J. Appl. Crystallogr.* **2000**, *33*, 1031.

42. Liu, K.; Zhang, L.; Liu, H.; Deng, P.; Du, H.; Li, X.; Zhang, J. *Mater. Lett.* **2013**, *90*, 145.

43. Li, L.; Li, C. Y.; Ni, C.; Rong, L.; Hsiao, B. *Polymer* **2007**, *48*, 3458.